

RESEARCH

Open Access



Manipulating subcellular protein localization to enhance target protein accumulation in minicells

Junhyeon Park¹, Karen M. Polizzi², Jongmin Kim³ and Juhyun Kim^{1*}

Abstract

Background Minicells are chromosome-free derivatives of bacteria formed through irregular cell division. Unlike simplified structures, minicells retain all cellular components of the parent cell except for the chromosome. This feature reduces immunogenic responses, making them advantageous for various biotechnological applications, including chemical production and drug delivery. To effectively utilize minicells, it is essential to ensure the accumulation of target proteins within them, enhancing their efficiency as delivery vehicles.

Results In this study, we engineered *Escherichia coli* by deleting the *minCD* genes, generating minicell-producing strains, and investigated strategies to enhance protein accumulation within the minicells. Comparative proteomic analysis revealed that minicells retain most parent-cell proteins but exhibit an asymmetric proteome distribution, leading to selective protein enrichment. We demonstrated that heterologous proteins, such as GFP and RFP, accumulate more abundantly in minicells than in parent cells, regardless of expression levels. To further enhance this accumulation, we manipulated protein localization by fusing target proteins to polar localization signals. While proteins fused with PtsI and Tsr exhibited 2.6-fold and 2.8-fold increases in accumulation, respectively, fusion with the heterologous PopZ protein resulted in a remarkable 15-fold increase in protein concentration under low induction conditions.

Conclusions These findings highlight the critical role of spatial protein organization in enhancing the cargo-loading capabilities of minicells. By leveraging polar localization signals, this work provides a robust framework for optimizing minicells as efficient carriers for diverse applications, from therapeutic delivery to industrial biomanufacturing.

Keywords Minicells, Polar localization, PopZ

Background

Bacteria are industrial workhorses for recombinant protein production, and advancements in synthetic biology enabled the engineering of genetic circuits to support various applications in healthcare, bioenergy, and environmental sustainability [1–5]. However, introducing engineered bacteria directly into real-world therapeutic or environmental settings raises significant safety concerns about unintended, uncontrolled propagation. Minicells, which are small vesicles produced through abnormal bacterial division, offer a safer alternative chassis. They retain all cellular components of their parent cells except chromosomal DNA [6, 7]. This unique

*Correspondence:

Juhyun Kim
juhyunkim@knu.ac.kr

¹ School of Life Sciences and Biotechnology, BK21 FOUR KNU Creative Bioresearch Group, Kyungpook National University, Daegu, Republic of Korea

² Department of Chemical Engineering and Imperial College Centre for Synthetic Biology, Imperial College London, London, UK

³ Department of Life Sciences, Pohang University of Science and Technology, Pohang 37673, Republic of Korea



© The Author(s) 2025. **Open Access** This article is licensed under a Creative Commons Attribution-NonCommercial-NoDerivatives 4.0 International License, which permits any non-commercial use, sharing, distribution and reproduction in any medium or format, as long as you give appropriate credit to the original author(s) and the source, provide a link to the Creative Commons licence, and indicate if you modified the licensed material. You do not have permission under this licence to share adapted material derived from this article or parts of it. The images or other third party material in this article are included in the article's Creative Commons licence, unless indicated otherwise in a credit line to the material. If material is not included in the article's Creative Commons licence and your intended use is not permitted by statutory regulation or exceeds the permitted use, you will need to obtain permission directly from the copyright holder. To view a copy of this licence, visit <http://creativecommons.org/licenses/by-nc-nd/4.0/>.

characteristic makes minicells particularly advantageous for various applications.

In bacteria, the Min system, comprising MinC, MinD, and MinE, regulates septum positioning by guiding FtsZ ring formation to the cell's midpoint. Disrupting this system induces minicell production [8, 9]. Briefly, the FtsZ ring forms at the midpoint to facilitate cell division with help from the MinCD complex, which inhibits FtsZ polymerization at the cell poles [10, 11]. MinE prevents the MinCD complex forming at the cell center, ensuring proper septum positioning for division [12]. Disruption of MinCD causes the FtsZ ring to assemble near cell poles, leading to minicell formation (Fig. 1A) [13]. Engineered minicells have shown promise in controlled biomolecule release and targeted drug delivery. For instance, immunization with minicells encapsulating the nucleoprotein triggered strong immune responses against lymphocytic choriomeningitis virus in animal models, demonstrating their

potential effectiveness as vaccines [14]. In addition, they can act as bioreactors for compound synthesis. Minicells derived from *Pseudomonas putida* can produce short-chain ketones from organic acids [15], and engineered *E. coli* minicells can synthesize toxic compounds that are typically difficult to produce in live bacterial cells [15, 16]. Furthermore, customized minicells with antibody surface modifications can target receptors overexpressed on cancer cells, enabling the delivery of therapeutic payloads exclusively to malignant cells while sparing healthy tissues [17]. While these applications are promising, a key challenge remains in concentrating target proteins within minicells to maximize their effectiveness across diverse applications. High protein concentrations are critical not only for therapeutic uses like enzyme replacement and targeted drug delivery but also for bioremediation, biosensing, and industrial bioproduction [18]. Engineering strategies to enhance protein localization and accumulation

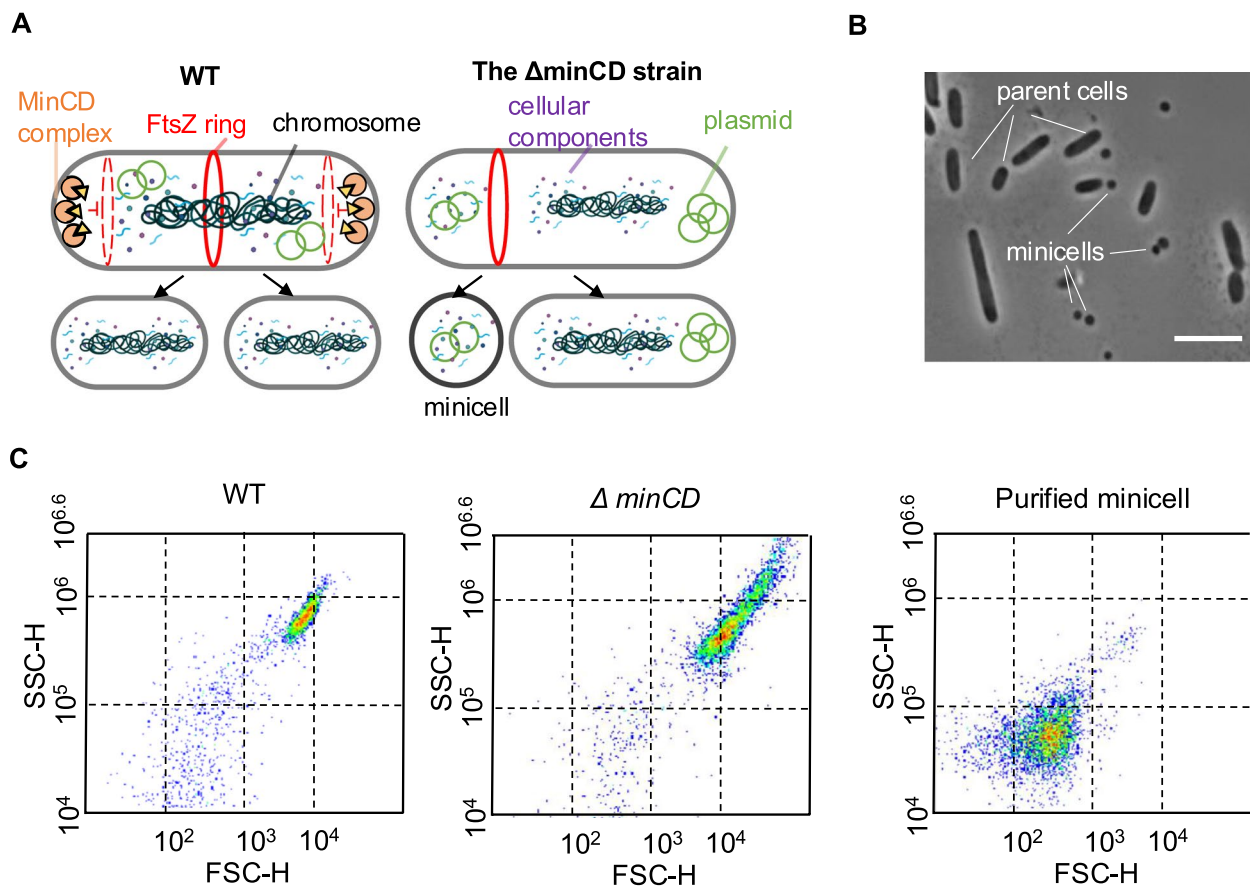


Fig. 1 Characterization of the Δ minCD strain. **A** The MinCD complex ensures symmetrical cell division by localizing properly at the cell poles. In its absence, irregular division occurs, leading to minicell formation. **B** Phase-contrast microscopy images of the Δ minCD strain. Cells grown overnight in LB were visualized using a phase-contrast microscope. Scale bar, 10 μ m. **C** Representative flow cytometry dot plots showing side scatter (SSC) versus forward scatter (FSC) for WT and Δ minCD strains. Cells were cultured overnight in LB, and more than 50,000 events were analyzed. Purified minicells were also included in the analysis

are essential to unlock the full potential of minicells as versatile tools in medicine, environmental sustainability, and biotechnology.

Despite lacking intracellular membranes, bacterial cells organize various components into specific subcellular regions, each with preferred localization patterns [19, 20]. This subcellular spatial organization means that minicells have a unique composition compared to their parent cells, potentially limiting the accumulation of target proteins in minicells [21, 22]. To address this, one approach involves manipulating protein localization. Previous research has demonstrated that linking GFP to ProP increases its accumulation in minicells. ProP serves as an osmosensory and osmoregulatory transporter that responds to changes in osmotic pressure [23, 24] and interacts with cardiolipin, which is enriched in minicells [16]. This observation prompted us to explore whether fusing the target protein directly to other localized molecules, similar to the GFP-ProP fusion, could also enhance its accumulation in minicells, or achieve this more efficiently.

To explore this, we engineered *E. coli* MG1655 by deleting the *minCD* genes, generating elongated parent cells and small, anucleate minicells. Our study focused on characterizing proteins enriched in minicells while also prioritizing the targeted accumulation of a specific protein in minicells. To achieve this, we compared the accumulation of heterologous proteins in minicells to that in parent cells and enhanced the concentration of the target protein by directing it to the cell poles. Specifically, we used polarly localized RNAs, such as ArcZ small RNA and fragmented *rpoS* mRNA, as well as proteins including PtsI, Tsr, and the heterologous PopZ. These macromolecules naturally localize to the cell poles in *E. coli* through distinct mechanisms, including biophysical forces, RNA–protein interactions, diffusion-and-capture processes, and membrane-associated cues [25–28]. Notably, fusing a fluorescent protein with the polar organizing protein PopZ substantially increased protein accumulation in minicells. These findings underscore the potential of targeted protein localization to enhance the cargo-loading capabilities of minicells, paving the way for efficient, compartmentalized bioproduction within minicells for a range of biotechnological applications.

Materials and methods

Culture conditions

Unless otherwise indicated, *E. coli* strains were grown at 37 °C in Luria–Bertani broth (LB; BD, Franklin Lakes, New Jersey, USA, Cat. No. 244620) with shaking at 180 rpm. Kanamycin (Km, 50 µg ml⁻¹), Ampicillin (Ap, 150 µg ml⁻¹), or Chloramphenicol (Cm, 30 µg ml⁻¹), was added to cultures of bacterial cells as needed to ensure

plasmid retention and maintenance of the manipulated genotype.

Cloning procedures and construction of reporter strains

The characteristics of the bacteria, plasmids, and primers used in this study are described in Supplementary Tables 1 and 2. DNA manipulation was carried out following a standard protocol [29]. Plasmid DNA was isolated from bacterial cells using the Exprep™ Plasmid SV mini Purification kit (GeneAll, Seoul, South Korea, Cat. No. 101–102). Restriction endonucleases were purchased from New England Biolabs (NEB). The *minCD*-deleted strain was constructed by replacing the target genomic regions with a kanamycin antibiotic cassette (pKD4) using the primers MinCD KO F/R, followed by the removal of the kanamycin resistance using the FLP recombinase according to a previously described method [29–31]. The gene deletion was confirmed using PCR (Check F/R), and the production of minicells from the genetically modified strain was observed.

To suppress the *minC* gene in *E. coli* MG1655, the pSECRi plasmid was modified to express a *minC*-specific single guide RNA (sgRNA) for CRISPR interference (CRISPRi) [38]. To this end, an overlap extension PCR was performed using primers (minC F/R) flanking the sgRNA expression site on the pSECRi plasmid. The PCR product was then treated with the DpnI enzyme for 1 h at 37 °C, followed by the purification of the newly synthesized DNA.

To create a reporter plasmid containing the sfGFP gene, PCR amplification was performed using pSEVA234-sfGFP [32] as a template and the sfGFP F/R primers. The amplified sfGFP gene was digested with *Bam*HI and *Hind*III, and the resulting fragments were ligated into pSEVA224 and pSEVA254 vectors, resulting in constructs pSEVA224::sfGFP and pSEVA254::sfGFP, respectively. Similarly, we cloned the mRFP gene into pSEVA234 by first amplifying it from pNNSCP [33] using the RFP F/R primers, and then digesting with *Avr*II and *Xba*I before ligation.

To manipulate the localization of reporter proteins, we created fusion constructs by combining either sfGFP or mRFP coding gene with molecules that target the cell poles. We generated transcriptional fusions by first amplifying either the *arcZ* gene or a fragment of the *rpoS* gene—both of which produce mRNAs that localize to the pole—using specific primer pairs (*arcZF*/R; *rposF*/R). After digesting both the amplified sequences and the pSEVA234::sfGFP plasmid with *Sac*I and *Eco*RI restriction enzymes, we ligated them together, resulting in the construction of pSEVA234::*arcZ*-sfGFP and pSEVA234::*rpoS*-sfGFP. In addition, we created translational fusion proteins by linking sfGFP to either the

C-terminal end of Tsr or PtsI as follows. Using the primer pairs tsrF/R and sfGFP linkF/sfGFP, amplicons of Tsr and sfGFP, including 3' and 5' flexible linker sequence overhangs complementary to each other, were obtained. These amplicons were then joined using SOEing PCR. The resulting PCR product was cloned into the pSEVA234 vector through *Bam*HI and *Hind*III restriction sites, followed by ligation, producing the construct pSEVA234::Tsr-sfGFP. Using the same method and primer pairs (PtsI F/R), we generated the PtsI amplicon and constructed pSEVA234::ptsI-sfGFP. We also cloned a PopZ fused mRFP module into the pSEVA234. The chimeric module was amplified using primer pairs (PopZ F/RFP R) containing the RBS_0034 coding sequence with the template plasmid pNNSCP [33]. The PCR product was then inserted into pSEVA234 using the restriction enzymes *Avr*II and *Xba*I, resulting in the plasmid pSEVA234::mRFP-PopZ.

All plasmid constructs were confirmed colony PCR using PE. coli DH5 α strain through transformation for DNA amplification. All experiments in this paper were performed in *E. coli* MG1655 Δ *minCD* after transformation with the corresponding plasmids.

Minicell purification and characterization

The overnight cultures of Δ *minCD* derivative strains were diluted 1:100 in 100 ml of fresh LB medium. For strains harboring isopropyl β -D-1-thiogalactopyranoside (IPTG; Sigma, St. Louis, Missouri, USA, Cat. No. I-6758)-inducible reporter constructs, protein expression was induced at this stage by adding IPTG at final concentrations of 5, 10, 20, or 50 μ M. The cultures were then incubated for an additional 16 h with agitation to promote minicell production. Minicells were isolated using a differential centrifugation protocol. The cultures were first centrifuged at 4000 \times g for 10 min to pellet the parental cells. The supernatant containing minicells was carefully collected and centrifuged again at 7197 \times g for 10 min to pellet the minicells. The resulting minicell pellet was resuspended and washed twice with phosphate-buffered saline (PBS) to remove residual growth medium and any contaminating parental cells. For final purification, the minicell suspension was passed through a 0.8- μ m size-exclusion membrane filter (Advantec, Taipei, Taiwan, Cat. No. 25CS080AS), effectively removing any remaining parental cell contaminants and yielding a highly enriched minicell preparation suitable for downstream analyses. The relative size of minicells and parent cells was determined using flow cytometry (Agilent, Santa Clara, California, USA, NovoCyte Advantec) based on forward scatter (FSC-H) and side scatter (SSC-H) parameters. Calibration was performed using size-standard beads (0.2, 0.4,

0.8, and 1 μ m) to estimate approximate cell dimensions. To reduce background noise, the SSC threshold was set to 1000 for all samples. Data acquisition was conducted at 50,000 events per sample, and dot plots were generated using the default software of the instrument.

We also carried out DAPI staining to determine the relative concentration of DNA in a cell. Either the rod-shaped parent cells or anucleate minicells were resuspended in 200 μ L of PBS including 4',6-diamidino-2-phenylindole (DAPI, 5 μ g/ml, All for Lab, Seoul, South Korea, Cat. No. 28718-90-3) and incubated at room temperature for 30 min. Following incubation, the samples were rinsed with PBS and analyzed using either fluorescent microscopy or flow cytometry with a Violet445 Pacific blue laser (561 nm/620 nm).

Microscopy and image analysis

Bacterial samples were immobilized by depositing them onto cover slips coated with poly-L-lysine (Sigma, St. Louis, Missouri, USA, Cat. No. P4707) and stored at room temperature to dry. The coverslip was then assembled with a slide glass containing the antifade reagent Prolong (Thermo Fisher, Waltham, Massachusetts, USA, Cat. No. P36984) and sealed with clear nail polish. The specimen was visualized using a fluorescence microscope. Microscopy was performed using an Olympus BX53F2 apparatus equipped with an 100 \times phase contrast objective and a FX900C camera of the same brand. Signals for GFP, DAPI, mRFP were obtained using wide field excitation with following filters; U-FFGFP, U-FFDAPI, U-FFTexas Red. The processing of multi-channel images was carried out using the software ImageJ.

Quantification of accumulation levels of reporter proteins

Reporter strains carrying reporter genes such as *sfGFP* and *mRFP* were pre-grown overnight in LB, and then the cultures were 100-fold diluted in the same medium containing IPTG at final concentrations of 0, 10, 50, 100, and 200 μ M. After induction, the samples were further cultured for 16 h, and fluorescence intensities were measured using a microplate reader (Synergy H1, Vermont, Winooski, USA, BioTek) at 488 /525 nm for GFP and at 545 /591 nm for RFP. To compare reporter expression levels between the parent cells and minicells, both cell populations were resuspended in PBS, and equal masses of cells, determined by OD_{600nm}, were analyzed using the microplate reader.

To estimate the intensities of sfGFP at the single-cell level, the suspension of cells in PBS was loaded into the flow cytometer and analyzed using blue laser (excitation 561 nm; emission 620/15 nm). For each sample, 50,000 events were analyzed, and population means were estimated using the default software of the instrument.

Western blot

Purified parent cells and minicells containing 100–400 μg of total protein were washed three times with PBS (DYNE BIO, Seoul, South Korea, Cat. No. CBP3070) to remove residual media and contaminants. The washed cell pellets were lysed using B-PER bacterial protein extraction reagent (Thermo Fisher Scientific, Waltham, Massachusetts, USA, Cat. No. 89821) following the manufacturer's protocol. The lysates were denatured by mixing with Laemmli sample buffer (Sigma, St. Louis, Missouri, USA, Cat. No. S3401) and heating at 95 °C for 5 min.

Protein samples were separated using sodium dodecyl sulfate–polyacrylamide gel electrophoresis (SDS-PAGE) on NuPAGE 4–15% TGX precast gels (Bio-Rad, Hercules, California, USA, Cat. No. 456–1084) in SDS-containing running buffer. Electrophoresis was performed at a constant voltage of 120 V for 90 min. The resolved proteins were transferred onto polyvinylidene difluoride (PVDF) membranes (All for Lab, Seoul, South Korea, Cat. No. 6872–25,025) at 100 V for 1 h using a wet-transfer system.

The membranes were blocked for 1 h at room temperature in Tris-buffered saline containing 5% skim milk and 0.1% Tween-20 (TBST) to minimize nonspecific antibody binding. After blocking, the membranes were incubated overnight at 4 °C with the primary antibody anti-GFP (Thermo Fisher Scientific, Waltham, Massachusetts, USA, Cat. No. PA5-109,258; diluted 1:4000 in 5% skim milk in TBST). Following the primary antibody incubation, membranes were washed three times for 10 min each with TBST and subsequently incubated with an HRP-conjugated goat anti-rabbit secondary antibody (Thermo Fisher Scientific, Waltham, Massachusetts, USA, Cat. No. 31460; diluted 1:5000 in 5% skim milk in TBST) for 1 h at room temperature. Excess secondary antibody was removed with three additional washes in TBST (10 min each).

Protein bands were visualized using the Pierce™ ECL Western Blotting Substrate (Thermo Fisher Scientific, Waltham, Massachusetts, USA, Cat. No. 32109), and chemiluminescent signals were captured using a Chemi-Doc Imaging System (ImageQuant™ LAS 500, Uppsala, Sweden). For GFP signal strength, internal control protein DnaK is used as a control to assess the relative protein abundance between minicells and parent cells.

Proteomics analysis

The ΔminCD strain was cultured overnight in LB and then separated into rod-shaped parent cell and anucleate minicell fractions. We extracted whole cellular proteins from an equal cellular masses in each fraction by lysing the cells using B-per buffer and sonication (vibra cell, CT Newtown, Pennsylvania, USA, US/VCX130PB).

The protein samples were mixed with 5x Laemmli buffer, vortexed thoroughly, and heated at 98 °C for 10 min to ensure protein denaturation. After a brief centrifugation, the samples were loaded onto SDS-PAGE gels composed of a 5% stacking gel and a 10% resolving gel. Electrophoresis was conducted at 60 V for stacking and 100 V for protein separation until the desired resolution was achieved. The gels were stained with InstantBlue® Coomassie Protein Stain (Abcam, Cambridge, England, Cat. No. ab119211) and subsequently stored in distilled water. Protein bands of interest were carefully excised from the gels and subjected to in-gel digestion. The gel pieces were destained with 30% ethanol at 60 °C, followed by sequential treatments with 50 mM ammonium bicarbonate (ABC)/50% acetonitrile (ACN), and 100% ACN to dehydrate the gels. Protein reduction was performed using 25 mM dithiothreitol (DTT) at 56 °C for 30 min, and alkylation was carried out with 55 mM iodoacetamide (IAA) in the dark for 30 min. The gel pieces were washed with 50 mM ABC, dehydrated with 100% ACN, and rehydrated with trypsin solution (Promega, Madison, Wisconsin, USA, Cat. No. V5111; 12.5 ng/ μL in 50 mM ABC). Digestion was performed at 37 °C for 16 h. Following digestion, peptides were extracted in 80% ACN/0.1% formic acid (FA) by vortexing and incubating for 15 min, and the supernatant was collected. The extraction process was repeated to maximize peptide recovery. The combined extracts were dried using a SpeedVac vacuum concentrator and reconstituted in 0.1% formic acid. The reconstituted peptide samples were centrifuged to remove particulates and prepared for LC–MS/MS analysis using a nano liquid chromatography–tandem mass spectrometry (Nano LC–MS/MS) system. Nano LC–MS/MS analysis was performed using the Ultimate 3000 system (Thermo fisher scientific, Waltham, Massachusetts, USA), with peptide separation carried out on a trap column (100 μm i.d., 150 mm, 100 Å, 5 μm) and an analytical column (75 μm i.d., 250 mm, 100 Å, 3 μm) at a flow rate of 0.3 $\mu\text{L}/\text{min}$ and 25 °C. Peptides were eluted using a gradient of solvent B (acetonitrile/0.1% formic acid) from 5 to 60% over 45 min. MS/MS analysis was conducted on a Q Exactive Plus mass spectrometer (Thermo fisher scientific, Waltham, Massachusetts, USA) in positive electrospray ionization (ESI+) mode, with full MS scans at 70,000 resolution (scan range: 150–2000 m/z) and data-dependent MS² (dd-MS²) scans using higher-energy collisional dissociation (HCD) at 35,000 resolution. The mass spectrometric data were processed with Proteome Discoverer (v2.5) software, and protein identification was performed against the *E. coli* reference database (UniProt ID 562). Label-Free Quantification (LFQ) was employed to determine relative protein abundance between samples.

Results and discussion

Production of minicells by disrupting the cellular division system

To generate anucleate minicells from the *E. coli* MG1655 strain, the MinCD complex-encoding genes were deleted using the lambda red recombination method (details in the Methods section), resulting in a minicell-producing strain. Microscopy analysis of the $\Delta minCD$ strain overnight grown in LB medium revealed the presence of both small spherical cells (minicells) and elongated rod-shaped cells, consistent with previous reports [9, 34] (Fig. 1B). To further characterize the $\Delta minCD$ strain, flow cytometry analysis was conducted. Both the wildtype (WT) and $\Delta minCD$ strains were cultured in LB medium until reaching the exponential phase ($OD \sim 0.5$) and analyzed based on their side and forward scatter properties. In agreement with the microscopy observations, the $\Delta minCD$ strain displayed a more heterogeneous population with varying cell lengths compared to the uniform rod-shaped WT cells. This heterogeneity arises from the random positioning of the FtsZ ring in the absence of MinCD (Fig. 1C). Minicells were separated from the rod-shaped parent cells through differential centrifugation, followed by purification through filtration (0.8 μm) (Fig. S1A). DAPI staining was used to distinguish nucleated parent cells from anucleate minicells. Flow cytometry analysis revealed significant DAPI signals in nucleated parent cells, but not in minicell (Fig. S1B). Microscopy analysis further confirmed the absence of DAPI signals in purified minicells, validating their anucleate nature (Fig. S1C). With this validation, we investigated the growth phase during which minicell production was predominant.

Minicells actively emerge from the minicell-producing strain during the exponential growth phase

Bacterial proteomes undergo significant changes as cells progress through different growth phases [35, 36]. During the exponential phase, proteins such as ribosomal proteins, metabolic enzymes, and those involved in DNA replication and cell division are highly abundant, whereas stress response proteins are predominantly upregulated in the stationary phase [37, 38]. Considering this, the proteins enriched within minicells could be influenced by their originating phase, as bacterial proteomes vary depending on the growth phase. To investigate this, we first determined the phase during which the majority of minicells emerge from the parent cell. To this end, we employed a CRISPR interference (CRISPRi) system to enable controlled suppression of cell division at different growth phases. We modified the pSECRi plasmid [39] to create pSECRi-minC, which targets the *minC* promoter region by the sgRNA along with the rhamnose inducible dCas9 protein (Fig. 2A) [40, 41]. This resultant plasmid

was then introduced into the MG1655 strain. Following an overnight culture of the transformed strain in LB with the inducer, microscopy analysis revealed a linear increase in the production level of small, sphere cells corresponding to the concentration of rhamnose (Fig. 2B). This suggests that inducible inhibition of transcription for the cell division system facilitated the formation of minicells. We also explored the induction of the CRISPRi system at different growth stages by introducing 5 mM of rhamnose at various phases of cell growth: at the initiation of the culture, during mid-exponential phases ($OD_{600\text{nm}}$ 0.2 or 0.4), and in the late exponential phase ($OD_{600\text{nm}} \sim 1.0$). Subsequently, all samples were cultivated for an additional 16 h to achieve maximum optical density across all tested conditions. Flow cytometry analysis, using clusters sorted by forward scattering to assess size of the parental and minicell populations, showed the highest fraction of minicells in the sample treated with rhamnose at the beginning of the culture compared to the other conditions (Fig. 2C). In contrast, lower minicell yields were observed when rhamnose was introduced during the mid-exponential phase, whereas minicell production dropped to minimal levels when the inducer was added in the late exponential phase, likely due to reduced division activity at this stage (Fig. 2C). These results suggest that proteins synthesized during the late exponential or stationary phase of the parent cells should not accumulate in minicells. Building on these observations, we further explored the proteomes specifically enriched in minicells.

Asymmetric distribution of the cellular proteome drives the enrichment of specific proteins in minicells

Bacterial proteins reside in specific subcellular regions, such as the cytoplasm, membrane, or poles [42, 43], through signal sequences including RNAs and peptides [44, 45]. As a result, bacterial subcellular architecture does not exhibit a symmetric distribution of the proteome, and the concentration of specific proteins can vary between parent cells and minicells. To decipher the distribution of the cellular proteome between these two populations, we conducted a comparative quantitative proteome analysis using Nano LC-MS/MS. The $\Delta minCD$ strain was cultured in LB overnight, and minicells were isolated as described above. Equal masses of the two cell types were used for the analysis. As a result, we identified a total of 1,367 and 1,368 proteins in parent cells and minicells, respectively, with only 22 and 23 proteins uniquely detected in each cell type (Fig. 3A). In total, these identified proteins represent 29.6% of all predicted protein-coding genes in the MG1655 strain [46], indicating that minicells largely contain the same proteins as their parent cells.

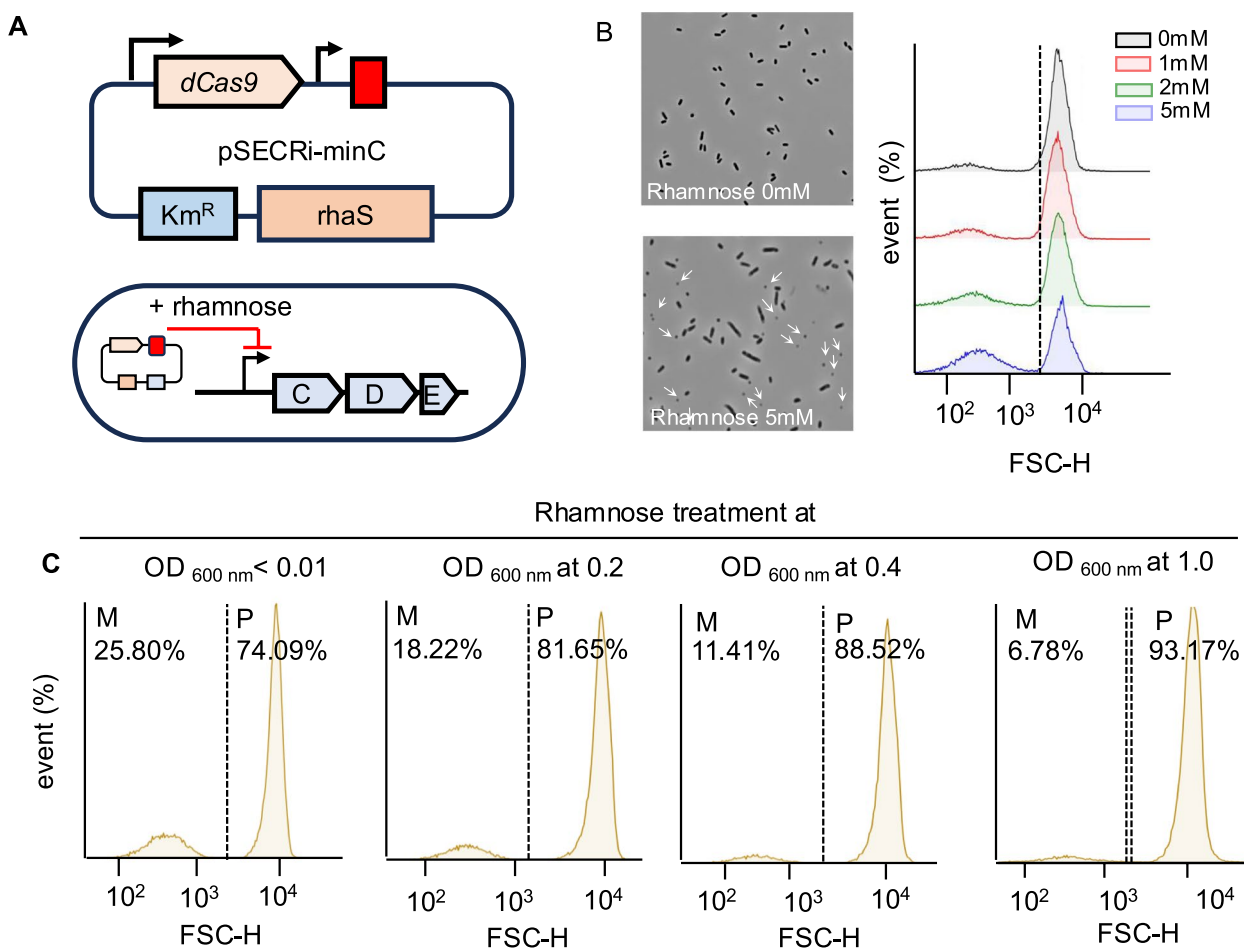


Fig. 2 Generation of minicells through transcriptional inhibition of the cellular division system. **A** Schematic representation of the transcriptional inhibition system using the CRISPRi plasmid (pSECRi). The pSECRi plasmid carries an sgRNA targeting the promoter regions of the *minCDE* genes in *E. coli*, enabling transcriptional repression. **B** Microscopy and flow cytometry analysis of CRISPRi-induced cells. Cells harboring the pSECRi plasmid were grown overnight in LB medium supplemented with varying concentrations of rhamnose to induce transcriptional inhibition. Samples were then either visualized using a phase-contrast microscope or analyzed by flow-cytometry to assess cell size. Rhamnose treatment is color-coded as follows: black for 0 mM, red for 1 mM, green for 2 mM, and blue for 5 mM. Scale bar, 5 μ m. **C** Inhibition of the division system at different growth phases. Cells harboring the pSECRi-minC plasmid were cultured in LB medium, and 5 mM rhamnose was added at various phases of cell growth. The cultures were further incubated for 16 h, and samples were analyzed using flow cytometry to quantify the minicell production rate. M denotes the minicell fraction, while P represents the parent cell fraction. Each fraction was sorted based on forward scattering to determine the sizes of the parent and minicell populations

We also compared the protein abundance in both cell types to determine the proteome configuration in minicells. By applying the criteria $|\text{fold-change}| > 2$ and $p < 0.05$, we identified 100 overrepresented proteins and 94 underrepresented proteins in the minicell fraction compared to parent cells (Fig. 3B). These 194 differentially expressed proteins were categorized into functional groups based on the Biological Process category [47]. The percentage for each functional category was calculated by dividing the number of proteins in the minicell fraction assigned to that category by the total number of proteins identified in both parent cells and minicells. The most

underrepresented group in minicells was associated with DNA and RNA metabolism (Fig. 3C). This result can be attributed to the gene expression architecture of the cell, as chromosomal DNA and the transcriptional machinery predominantly reside in the nucleoid located at central regions of the cell [48, 49], with fewer cellular components accumulating at the cell poles, influencing the proteome distribution in minicells. However, this does not imply that minicells lack gene expression capacity. A previous study demonstrated that anucleate minicells carrying circuit genes responded to inducers by exhibiting reporter activity, highlighting their potential to serve

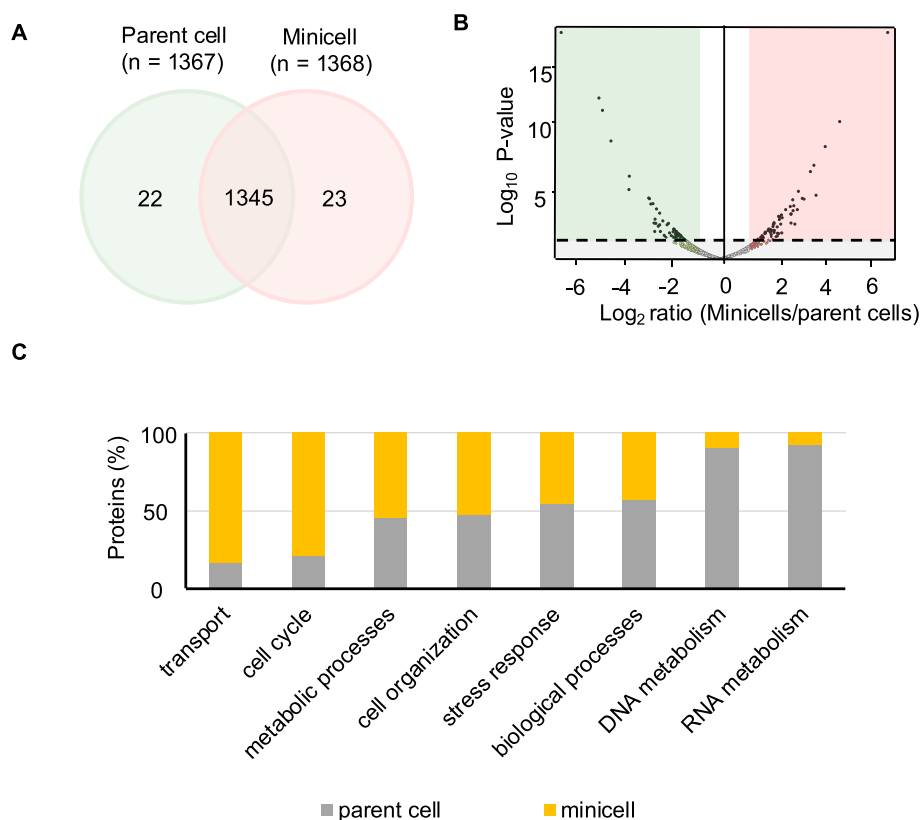


Fig. 3 Comparative proteomics analysis of *E. coli* parent cells and minicells. **A** Venn diagram illustrating the overlap and unique distribution of identified proteins between *E. coli* parent cells and minicells. A total of 1345 proteins were shared between the two populations, while 22 proteins were uniquely detected in parent cells and 23 in minicells. **B** Volcano plot depicting the differential abundance of proteins in minicells and parent cells. The x-axis represents Log_2 [fold-change], where fold-change = abundance of minicells / abundance of parent cells, and the y-axis denotes $-\text{Log}_{10}$ [p -value]. Proteins significantly enriched in parent cells are shown in green (Log_2 [fold-change] < -1), while those enriched in minicells are displayed in red (Log_2 [fold-change] > 1). The dashed horizontal line indicates the significance threshold (p -value < 0.05). **C** Functional categorization of proteins based on enrichment in parent cells (gray) and minicells (yellow). Categories include transport, cell cycle, metabolic processes, cell organization, stress response, biological processes, DNA metabolism, and RNA metabolism. Bars represent the proportion of proteins identified within each functional category

as chassis for functional biosensors [50, 51]. On the other hand, a group related to transport was the most upregulated in minicells (Fig. 3C). It is known that the majority of cellular activities in bacterial cell poles involve active transport and chemotaxis [52], providing support for our proteomic analysis in profiling protein subsets in minicells.

Heterologous proteins accumulate more abundantly in minicells than in parent cells

We then examined the accumulation levels of heterologous proteins in minicells, a key factor for various biotechnological applications. To achieve this, we introduced an IPTG-inducible GFP construct, pSEVA234-*sfgfp*, into the Δ *minCD* strain. The reporter strain, capable of producing minicells, was cultured overnight in LB supplemented with 50 μM IPTG. Parent cells and minicells were then separated from the culture, and

whole cellular proteins were extracted from equal masses of each fraction. The relative accumulation of fluorescent proteins between parent cells and minicells was subsequently analyzed through western blotting using an anti-GFP antibody. The results showed that GFP signals were more prominent in the minicell fraction compared to the parent cells, whereas DnaK expression levels remained consistent across both fractions (Fig. 4A). Previous studies have reported higher accumulation levels of certain recombinant proteins, such as hemagglutinin (HA) and GFP, in minicells [22]. This suggests that minicells may serve as passive reservoirs for proteins that are overproduced or lack active retention signals in the parent cell. We also quantified accumulation level of the fluorescent protein in each fraction with a microplate reader at different levels of IPTG induction (Fig. 4B). Consistent with the western blot analysis, the OD-normalized value of GFP was enriched twofold in minicells relative to parental

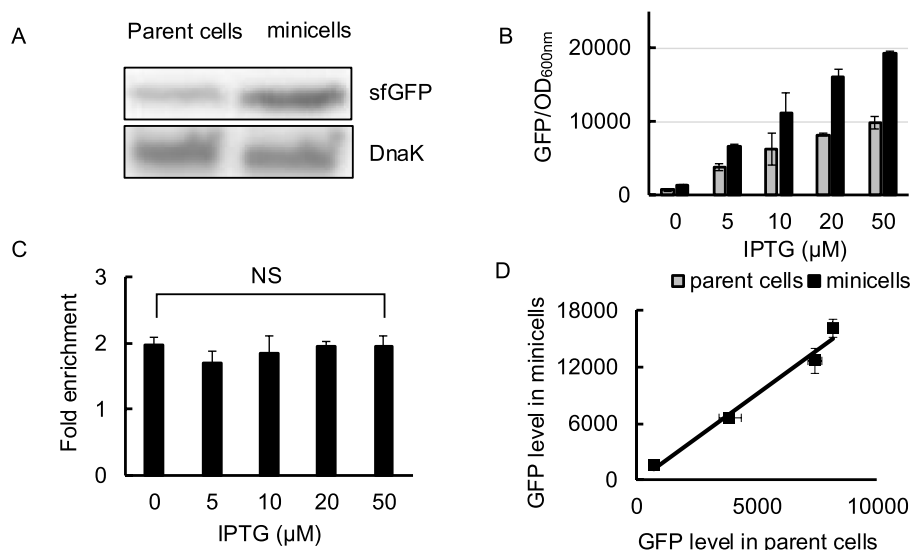


Fig. 4 Quantitative analysis of sfGFP expression and enrichment in *E. coli* parent cells and minicells. **A** The $\Delta minCD$ strain harboring pSEVA234-sfGFP was cultured overnight in LB medium with 50 μ M IPTG. Parent cells and minicells were isolated from the culture, and whole-cell proteins were extracted from equal masses of each fraction. The relative accumulation of fluorescent proteins in parent cells and minicells was analyzed through western blot using an anti-GFP antibody, with DnaK serving as the loading control. **B** The reporter strain was also cultured with varying concentrations of IPTG (0, 5, 10, 20, and 50 μ M), and the fluorescence intensities were measured in both isolated parent cells and minicells. **C** The fluorescence signals from each fraction were used to estimate the relative enrichment of the reporter protein in minicells compared to parent cells, expressed as fold enrichment. Fold enrichment in minicells is calculated as the fluorescence intensity in minicells divided by that in parent cells. No significant (NS) fold enrichment was observed, regardless of the GFP expression level in parent cells. **D** Correlation of GFP accumulation between parent cells and minicells. Error bars represent mean \pm SD ($n=3$), ($R^2=0.9937$)

cells (Fig. 4C). Furthermore, although GFP expression levels increased in parent cells, the relative fold-enrichment in minicells remained consistent (Fig. 4D). Notably, this is not the result of GFP synthesis in minicells. When minicells were purified from the reporter strain grown in LB and incubated with varying concentrations of IPTG for 12 h, no dramatic increase of GFP accumulation in minicells was detected (Fig. S2). Therefore, most of the GFP originated from the parent cells and entered the minicell during division. When the reporter protein was switched from GFP to monomeric RFP (mRFP), a similar phenomenon was observed. Regardless of the protein expression level in parent cells, mRFP showed approximately twofold enrichment in minicells (Fig. S3A). This suggests that the identity of the reporter protein is not the key factor driving its distribution. Instead, such non-essential proteins may preferentially accumulate at the poles due to non-uniform distribution within the cell, potentially influenced by volume exclusion effects caused by chromosomal DNA [53]. We also cannot rule out the possibility that the higher accumulation of fluorescent proteins in minicells is, at least in part, due to a cellular strategy for expelling unwanted protein aggregates. In *E. coli*, the small heat shock protein IbpA [54], which binds to misfolded and aggregated proteins, has been shown to associate with inclusion bodies and facilitate their

sequestration [55]. Notably, Rang et al. reported that fluorescently labeled IbpA was predominantly detected in minicells under antibiotic-induced stress conditions, suggesting that minicells function as a damage disposal mechanism to help bacterial cells manage proteotoxic stress [56]. This phenomenon could provide an additional explanation for our observations, where certain proteins—such as GFP—are enriched in minicells relative to the parent cells.

To further examine the protein-capturing capacity of minicells, we cloned the sfGFP coding gene into plasmids with different origins of replication, such as RK2 and RSF1010, resulting in low and high gene dosage, respectively. Ultimately, three different reporter plasmids, pSEVA224-, pSEVA234-, and pSEVA254-sfgfp, were used (Fig. S4A) to quantify the accumulation level of the fluorescent protein based on gene dosage in the minicell-producing strain. All the reporter strains were cultured in LB with varying concentrations of IPTG overnight. After separating the parent cell and minicell fractions as described earlier, GFP intensities in each sample were analyzed at the single-cell level using flow cytometry. Interestingly, GFP expression levels increased in both parent cells and minicells with higher gene dosage and elevated IPTG concentrations (Fig. S4B). The highest GFP accumulation was observed in both fractions

when the high-copy-number plasmid was combined with 50 μ M IPTG treatment in the culture (Fig. S4B). This suggests that an increase in heterologous protein production in parent cells leads to a proportional accumulation in minicells. It is worth noting that GFP intensities in minicells were approximately 10 times lower than in parent cells at the single-cell level (Fig. S4C), likely due to the difference in cell volume between parent cells and minicells. Another possible explanation is asymmetric protein partitioning during cell division, which may lead to an uneven distribution of specific proteins within the cell [57]. While such partitioning may have some influence on protein distribution, our data do not conclusively support it as the main factor determining reporter levels in minicells. Instead, the higher GFP or RFP concentration per unit volume in minicells suggests that these vesicle-like structures may have an enhanced ability to retain or accumulate proteins compared to parent cells. This could be attributed to differences in protein diffusion dynamics, membrane retention, or cellular physiology. Accordingly, these findings highlight the potential of minicells as efficient protein carriers, as they can retain high concentrations of proteins produced by their parent cells. Building on the ability of anucleate minicells to effectively encapsulate valuable products for various biotechnological applications, we engineered them to maximize the accumulation of the target protein.

Manipulating the spatial distribution of target protein can enhance its accumulation in minicells

Since minicells originate from the polar region of the parent cell, we hypothesized that the accumulation of a heterologous protein in minicells could be enhanced by directing the spatial localization of the target protein to the cell poles. As previously discussed, cellular proteomes exhibit asymmetric distribution, with certain proteins specifically localized at the cell poles [26, 58]. Several studies have demonstrated that asymmetric protein segregation is a key strategy for bacteria to manage damaged or toxic proteins [55–57, 59, 60]. During cell division, these proteins tend to accumulate preferentially in one daughter cell, leading to distinct physiological outcomes. This process plays a critical role in bacterial aging and rejuvenation, where one daughter cell inherits a higher burden of damaged proteins and experiences proliferative mortality, while the other, largely free from these accumulations, is effectively rejuvenated and retains its replicative potential. This segregation mechanism ensures that at least a subset of the bacterial population remains physiologically younger and more fit for continued growth and adaptation. It is established that aging-related protein aggregates localize to the cell center and poles in *E. coli* due to the interplay between passive

diffusion-aggregation and spatially non-homogeneous macromolecular crowding, which results from nucleoid organization [60].

While passive mechanisms such as diffusion and crowding effects contribute to protein segregation, bacteria also employ active mechanisms to facilitate protein localization to the poles [61]. For instance, RNAs contribute to the enrichment of their encoded proteins at the cell poles and outside the nucleoid regions. This may be attributed to either the “ZIP code” sequence of the transcripts [62] or the cytoplasmic property as RNAs longer than 500 nucleotides have difficulty penetrating the densely packed DNA within the nucleoid [63]. In addition, several small RNAs, including ArcZ, are highly concentrated at the cell poles, where they regulate target molecules that are enriched in these regions [25]. Polarly localized proteins are directed to the poles through interactions with pre-existing proteins or protein complexes at these sites, known as the diffusion-and-capture mechanism [26, 64]. Physical force induced by nucleoid exclusion facilitates the distribution of proteins at the pole [65, 66], and differences in membrane and cell envelope composition, including the enrichment of anionic phospholipids like cardiolipin at the poles, further serve as cues for polar localization [67]. ProP is responsible for interacting with cardiolipin, and GFP fused to ProP was previously detected at cell poles [68]. When this fusion protein is introduced into minicell-producing cells, the fluorescence intensities increase in minicells by 58% compared to non-linked GFP [16]. However, a recent study demonstrated that the interaction between MinD and RNase E is crucial for the proper localization of polar mRNAs. In the absence of MinD, RNase E improperly degrades polar mRNAs, such as *prop* [69]. This highlights the importance of identifying and utilizing alternative molecules that can localize to the cell poles independently of MinD, as a strategy to enhance the accumulation of specific proteins in minicells.

To achieve this, we engineered the *gfp* cargo by fusing it with polar localization molecules (Fig. 5A). The initial factor considered was RNA signals, and the *gfp* gene was transcriptionally fused to either the polarly localized ArcZ small RNA or a segment of *rpoS* mRNA. The transcription fusion was constructed using pSEVA234, and the reporter plasmids were introduced into the Δ *minCD* strain. After growing the strains in LB containing 10 μ M IPTG overnight, we separated parent cells and purified the minicell fraction to measure the GFP intensity in each fraction. These two transcriptional fusions, however, did not significantly increase the fold enrichment of GFP accumulation in minicells (Fig. 5B), likely due to the non-spatial distribution of the fusion products (Fig. S5). The second factor we considered was the polar

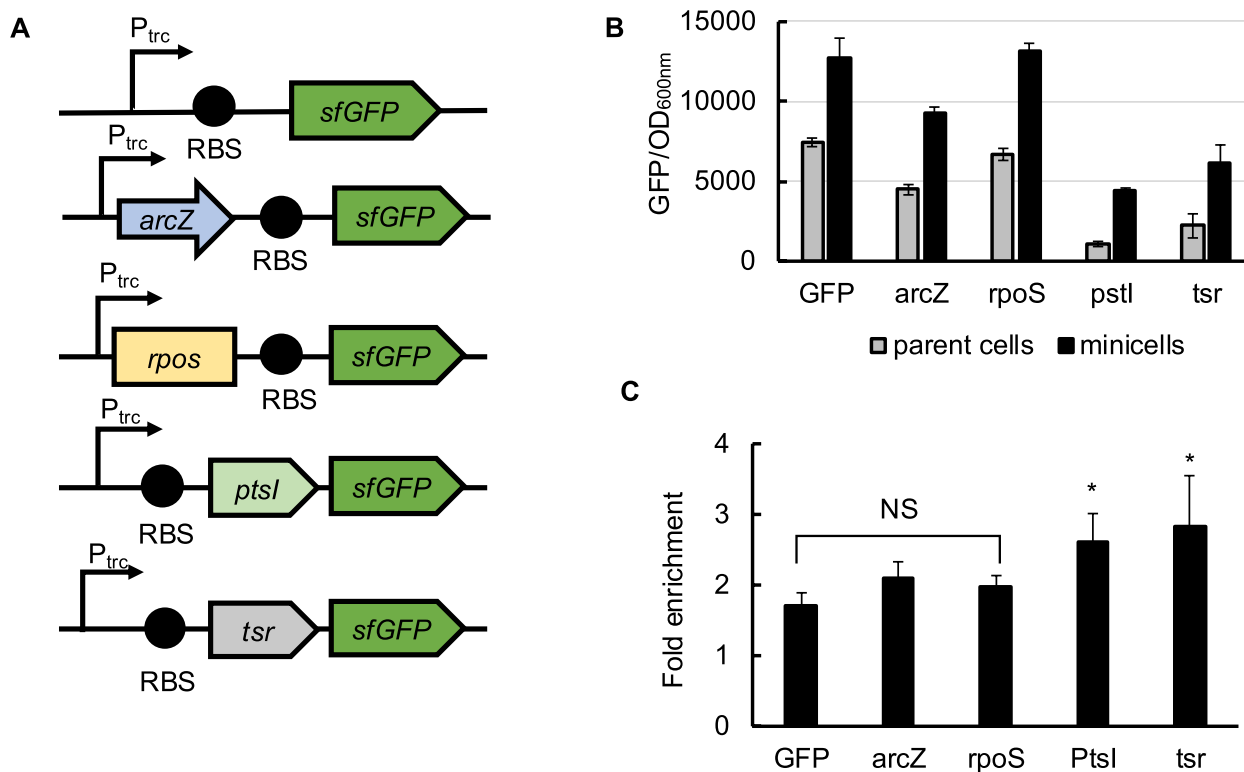


Fig. 5 Engineering of the spatial distribution of reporter protein using polar localization signals. **A** Schematic representation of constructs designed to enable the potential repositioning of the reporter protein. Polarly localized RNA elements, ArcZ sRNA and segmented rpoS mRNA, were transcriptionally fused to the reporter gene. Translational fusions with proteins exhibiting polar localization, PtsI and Tsr, were also included. **B** Reporter strains carrying different fusion constructs were cultured in the presence of 10 μ M IPTG, and fluorescence intensities were measured in isolated parent cells and minicells. **C** The fluorescence signals from (B) were analyzed to evaluate the relative enrichment of the reporter protein in minicells compared to parent cells. Fold enrichment in minicells is calculated as described in Fig. 4C. Error bars represent the mean \pm standard deviation ($n=3$), ns; not significant; * $P < 0.1$, compared to the non-fusion condition

localization proteins identified in *E. coli*. Previous studies have shown that both PtsI and Tsr predominantly localize at the cell poles [27, 70]. PtsI is involved in sugar uptake and phosphorylation, while Tsr, a critical component of the chemotaxis system, senses serine gradients and other environmental cues [28, 71]. When these proteins were translationally fused with GFP at their C-terminus, we observed fluorescent foci in the polar regions of minicell-producing parent cells (Fig. S5). Using the same procedure applied to study the effect of RNA signals, the relative accumulation levels of GFP expression were analyzed between parent cells and purified minicells. Although the translational fusion led to a lower expression level of the reporter, the spatial distribution driven by the polar localization proteins resulted in a 62% and 75% increase in fold enrichment levels in minicells for PtsI and Tsr, respectively (Fig. 5C). It is important to note that the fusion proteins were not exclusively localized to the cell poles; they were also spatially distributed within the cytosolic and membrane regions, consistent with their functional roles (Fig. S4). This incomplete

polar localization could result in suboptimal concentrations of target proteins in minicells.

The limited success of RNA-based localization signals and the incomplete polar localization of PtsI and Tsr suggest that multiple factors influence protein targeting in minicells. Polarly localized RNAs like ArcZ and rpoS mRNA may have been ineffective due to degradation, weak interactions with localization machinery, or the absence of MinD, which stabilizes polar mRNAs. Similarly, PtsI and Tsr, despite their natural enrichment at the poles, did not localize exclusively when fused to GFP, likely due to their intrinsic functions, diffusion-and-capture mechanism, and structural constraints. These findings illustrate the complexity of protein localization and suggest the need for alternative strategies. In response, we explored a heterologous polar localization signal to evaluate its potential for enhancing target protein accumulation in minicells.

Engineering protein localization to the old pole boosts the accumulation of target proteins in minicells

Caulobacter PopZ is a naturally occurring, polar-localized protein that plays a crucial role in cell division and interacting with ParB-parS complexes. [66, 72]. When expressed in *E. coli*, the protein also localizes to the old cell pole, predominantly at a single pole [53, 73]. However, PopZ accumulates at both poles when overexpressed, resulting in a bipolar distribution [73, 74]. This localization is driven by self-oligomerization and potential protein–protein interactions [75, 76]. Additionally, the intrinsically disordered regions at the N-terminus have been shown to interact with pole-specific proteins in *C. crescentus*, suggesting that similar interactions may occur in *E. coli*, facilitating PopZ localization to the poles [76, 77]. This polar localization characteristic can be utilized to target proteins to specific subcellular regions, particularly cell poles, which may enhance their accumulation in purified minicells. To explore this potential, we created a DNA construct encoding the fusion of the N-terminus of PopZ to mRFP [33] and introduced the plasmid carrying the chimera reporter into the Δ *minCD* strain. To ensure comparability and to maintain the original functional and localization characteristics, we opted to retain the previously established RFP fusion

for PopZ (Fig. 6A). Although the reporter strain carrying the *mRFP-PopZ* module was cultured in LB without an inducer, fluorescence signals were still detectable due to leaky expression, with most foci localized to a single pole (Fig. 6B). Notably, when the relative accumulation between parent cells and purified minicells was analyzed, a remarkable 15-fold increase in fold enrichment was observed (Fig. 6C). Upon treatment with IPTG, a higher level of fusion protein accumulation was observed, this time at both poles of the parent cells, and this bipolar localization gradually extended from the poles into the cytoplasmic space according to the level of inducer concentration (Fig. 6D). This suggests a spatial constraint in capturing proteins at the cell poles. As expected, the subcellular architecture of protein distribution resulted in relatively lower accumulation of the reporter protein in minicells compared to parent cells as the expression level of RFP-PopZ increased (Fig. 6C). Nevertheless, the fluorescence signals in minicells intensified proportionally with the inducer concentration (Fig. 6B). These results strongly indicate that manipulating protein distribution at cell poles, which are potentially minicell-producing sites, enables the enrichment of proteins in minicells. The H3H4 domain of PopZ is critical for its spatial localization and interactions with other proteins [75], suggesting

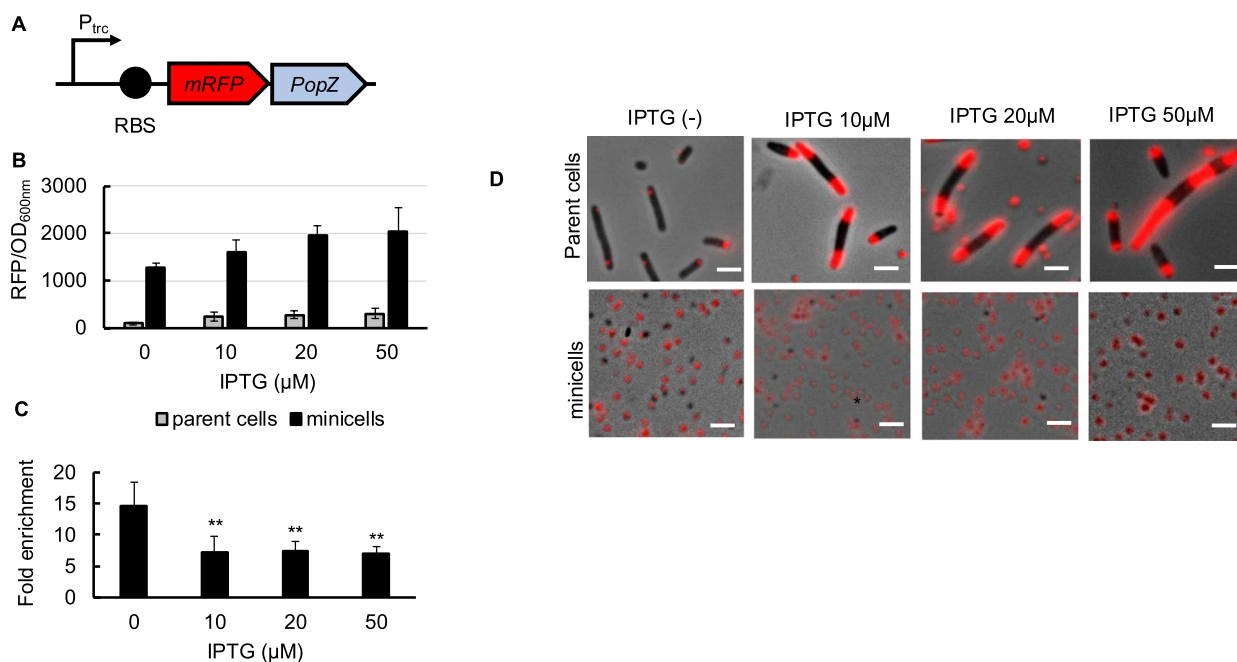


Fig. 6 PopZ protein-mediated positioning of the reporter protein in minicells. **A** Schematic representation of the IPTG inducible mRFP-PopZ construct. **B** The reporter strain, carrying the PopZ fusion, was cultured with varying concentrations of IPTG (0, 10, 20, and 50 μ M). The fluorescence intensities were measured in both isolated parent cells and minicells. **C** The RFP signals from each fraction were used to estimate the fold enrichment of the reporter protein in minicells compared to parent cells. Error bars represent mean \pm SD ($n=3$), ** $P < 0.05$, compared to the no IPTG treated condition. **D** The localization of the PopZ-RFP fusion protein was visualized in both parent cells and minicells through microscopy. Images were captured in phase contrast and fluorescence channels and merged using ImageJ. Scale bars, 10 μ m

that fusing proteins with this essential domain may be sufficient to modulate their distribution in bacteria. This engineering approach will serve as a framework to enhance the accumulation of desired proteins in minicells as functional cellular chassis for diverse biotechnological applications.

Conclusions

This study demonstrates the engineering of minicells derived from *E. coli* to enhance the accumulation of target proteins by manipulating subcellular protein localization. By disrupting the MinCD complex, we generated minicell-producing strains and comprehensively characterized the unique proteome distribution in minicells in comparison to parent cells. We found that minicells predominantly contained proteins synthesized by their parent cells, with specific enrichment and depletion patterns reflecting an asymmetric proteome distribution. Importantly, heterologous proteins were found to accumulate more abundantly in minicells than in parent cells, emphasizing their potential as protein carriers. Based on these observations, we explored strategies to further enhance protein accumulation in minicells by directing the spatial distribution of target proteins to cell poles. Translational fusions with PtsI and Tsr led to moderate increases in protein enrichment within minicells, while PopZ proved to be the most effective, achieving up to a 15-fold enhancement. These findings demonstrate the critical role of spatial arrangement in maximizing the efficiency of protein accumulation within minicells. By leveraging polar localization signals, we provide a robust framework for increasing the efficiency of minicells in concentrating target proteins, paving the way for their more effective use in synthetic biology and industrial biotechnology. Future research could expand on these findings by exploring additional localization signals, refining minicell engineering strategies, and testing their applicability in broader industrial and therapeutic settings.

Abbreviations

LB	Luria–Bertani broth
Km	Kanamycin
Amp	Ampicillin
Cm	Chloramphenicol
sgRNA	Single guide RNA
CRISPRi	CRISPR interference
IPTG	Isopropyl β-D-1-thiogalactopyranoside
PBS	Phosphate-buffered saline
DAPI	4',6-Diamidino-2-phenylindole
PVDF	Polyvinylidene difluoride
ABC	Ammonium bicarbonate
ACN	Acetonitrile
DTT	Dithiothreitol
IAA	Iodoacetamide IAA
FA	Formic acid
ESI+	Positive electrospray ionization
dd-MS ²	Data-dependent MS ²
HCD	Higher-energy collisional dissociation

LFQ Label-Free Quantification
mRFP Monomeric RFP (mRFP)

Supplementary Information

The online version contains supplementary material available at <https://doi.org/10.1186/s13036-025-00495-y>.

Supplementary Material 1: Table S1. Bacterial strains, plasmids used for this study. Table S2. Primers used in this study.

Supplementary Material 2: Fig. S1. Characterization of minicells isolated from the $\Delta minCD$ strain. (A) Representative images showing the overnight culture of the minicell-producing strain, initial minicell purification through centrifugation, and further purification using a 0.8- μ m filter. Scale bar, 5 μ m. (B) Flow cytometry analysis of DAPI-stained samples to evaluate DNA content. Pacific Blue fluorescence intensity profiles are shown for WT cells, $\Delta minCD$ cells, and purified minicells. The $\Delta minCD$ strain exhibited a distinct population of chromosome-free minicells with lower fluorescence intensity compared to the chromosome-containing WT strain. (C) Samples were visualized using fluorescence microscopy. Phase contrast and DAPI fluorescence images were captured and merged using ImageJ. Scale bars, 10 μ m. Fig. S2. Induction of the reporter gene in purified minicells. (A) Schematic representation of the experimental workflow. The minicells carrying the reporter plasmid pSEVA234-sfGFP were isolated from the overnight culture of the $\Delta minCD$ strain. (B) The minicell sample was incubated with varying concentrations of IPTG (0, 10, and 50 μ M) for 16 h, and fluorescence intensity was measured to quantify sfGFP expression. Results are presented as mean \pm standard deviation ($n = 3$), ** $P < 0.01$, compared to the no IPTG treated condition. Fig. S3. Distribution of mRFP in a minicell-producing strain. (A) The $\Delta minCD$ strain carrying the mRFP system was grown in LB with varying concentrations of IPTG (0, 5, 10, 20, and 50 μ M), and the fluorescence intensities were measured in both isolated parent cells and minicells. The fluorescence signals obtained from each fraction were used to estimate the fold enrichment of the reporter protein in minicells compared to parent cells. No significant (NS) fold enrichment was detected, regardless of the RFP accumulation level in parent cells. (B) Upon induction with 50 μ M IPTG, two types of cells were observed using fluorescence microscopy, and mRFP signals were uniformly distributed throughout the cytoplasm of parent cells. Scale bars, 10 μ m. Fig. S4. Evaluation of protein-capturing capacity of minicells. (A) Schematic representation of plasmids carrying the sfGFP reporter gene under the control of an IPTG-inducible promoter. Plasmids with different origins of replication were used: RK2 (pSEVA224), pBBR1 (pSEVA234), and RSF1010 (pSEVA254). (B) GFP fluorescence intensities were measured in parent cells (left) and minicells (right) for strains carrying the indicated plasmids. The cells were grown in the presence of varying concentrations of IPTG (0, 5, 10, 20, and 50 μ M). Error bars represent mean \pm SD ($n = 3$). Fig. S5. Spatial distribution of the reporter protein fused to a particular signal. Reporter strains described in Figure 5 were cultured in LB with IPTG, and the localization of the reporter protein was observed using a fluorescence microscope. Arrows in the merged images indicate polar enrichment and specific localization patterns. Phase contrast, GFP (green), and composite images are shown. Scale bars, 10 μ m.

Acknowledgements

The authors are indebted to Dr. Daehee Lee (Korea research institute of bioscience and biotechnology) for the pSECRi plasmid. We extend our gratitude to Geonhu Lee for the insightful discussions.

Authors' contributions

J.P., K.P., J.K. and J.K. conceived and designed the research. J.P. carried out the experiments and respective analyses. All authors wrote the manuscript.

Funding

This work was supported by the National Research Foundation of Korea (NRF) grant funded by the Ministry of Science and ICT (2022R1A2C1006157, 2022R1A4A1025913, RS-2024-00439872), the Korea Health Technology R&D Project through the Korea Health Industry Development Institute (KHIDI), funded by the Ministry of Health & Welfare, Republic of Korea

(RS-2023-00304637), and the UKRI through the EPSRC Adventurous Manufacturing Programme (EP/T005297/1, EP/W00979X/1).

Data availability

No datasets were generated or analysed during the current study.

Declarations

Ethics approval and consent to participate

Not applicable.

Consent for publication

Not applicable.

Competing interests

The authors declare no competing interests.

Received: 3 February 2025 Accepted: 17 March 2025

Published online: 29 March 2025

References

- Chang M, Ahn SJ, Han T, Yang D. Gene expression modulation tools for bacterial synthetic biology. *Biotechnology for Sustainable Materials*. 2024;1(1):6.
- Sarethy IP, Saxena Y, Kapoor A, Sharma M, Sharma SK, Gupta V, et al. Alkaliphilic bacteria: applications in industrial biotechnology. *J Ind Microbiol Biotechnol*. 2011;38(7):769.
- Korc E, Varga L. *Exopolysaccharides* from lactic acid bacteria: Technofunctional application in the food industry. *Trends Food Sci Technol*. 2021;110:375–84.
- Sasaki K, Watanabe M, Suda Y, Ishizuka A, Noparatnaraporn N. Applications of photosynthetic bacteria for medical fields. *J Biosci Bioeng*. 2005;100(5):481–8.
- Shende P, Basarkar V. Recent trends and advances in microbe-based drug delivery systems. *Daru-Journal of Pharmaceutical Sciences*. 2019;27(2):799–809.
- Clowes RC. Molecular structure of bacterial plasmids. *Bacteriol Rev*. 1972;36(3):361–405.
- Jaffe A, D'Ari R, Hiraga S. Minicell-forming mutants of *Escherichia coli*: production of minicells and anucleate rods. *J Bacteriol*. 1988;170(7):3094–101.
- Bi E, Lutkenhaus J. FtsZ Ring Structure Associated with Division in *Escherichia-Coli*. *Nature*. 1991;354(6349):161–4.
- Lutkenhaus J. Assembly dynamics of the bacterial MinCDE system and spatial regulation of the Z ring. *Annu Rev Biochem*. 2007;76:539–62.
- Szwedziak P, Ghosal D. FtsZ-ring architecture and its control by MinCD. *Prokaryotic Cytoskeletons: Filamentous Protein Polymers Active in the Cytoplasm of Bacterial and Archaeal Cells*. 2017:213–44.
- Fu X, Shih Y-L, Zhang Y, Rothfield LI. The MinE ring required for proper placement of the division site is a mobile structure that changes its cellular location during the *Escherichia coli* division cycle. *Proc Natl Acad Sci*. 2001;98(3):980–5.
- Farley MM, Hu B, Margolin W, Liu J. Minicells, Back in Fashion. *J Bacteriol*. 2016;198(8):1186–95.
- Giacalone MJ, Zapata JC, Berkley NL, Sabbadini RA, Chu Y-L, Salvato MS, et al. Immunization with non-replicating *E. coli* minicells delivering both protein antigen and DNA protects mice from lethal challenge with lymphocytic choriomeningitis virus. *Vaccine*. 2007;25(12):2279–87.
- Kozaeva E, Nieto-Dominguez M, Tang KKY, Nikel PI. Leveraging engineered *Pseudomonas putida* minicells for bioconversion of organic acids into short-chain methyl ketones. *bioRxiv*. 2024:2024.01.06.574483.
- Kim S-J, Chang W, Oh M-K. *Escherichia coli* minicells with targeted enzymes as bioreactors for producing toxic compounds. *Metab Eng*. 2022;73:214–24.
- Solomon BJ, Desai J, Rosenthal M, McArthur GA, Pattison ST, Pattison SL, et al. A first-time-in-human phase I clinical trial of bispecific antibody-targeted, paclitaxel-packaged bacterial minicells. *PLoS ONE*. 2015;10(12):e0144559.
- Ali MK, Liu Q, Liang K, Li P, Kong Q. Bacteria-derived minicells for cancer therapy. *Cancer Lett*. 2020;491:11–21.
- Govindarajan S, Amster-Choder O. Where are things inside a bacterial cell? *Curr Opin Microbiol*. 2016;33:83–90.
- Surovtsev IV, Jacobs-Wagner C. Subcellular organization: a critical feature of bacterial cell replication. *Cell*. 2018;172(6):1271–93.]
- Shen H, Aggarwal N, Wun KS, Lee YS, Hwang IY, Chang MW. Engineered microbial systems for advanced drug delivery. *Adv Drug Deliv Rev*. 2022;187:114364.
- Yu H, Khokhlatchev AV, Chew C, Illendula A, Conaway M, Dryden K, et al. Minicells from highly genome reduced *Escherichia coli*: cytoplasmic and surface expression of recombinant proteins and incorporation in the minicells. *ACS Synth Biol*. 2021;10(10):2465–77.
- Tsatskis Y, Khambati J, Dobson M, Bogdanov M, Dowhan W, Wood JM. The osmotic activation of transporter ProP is tuned by both its C-terminal coiled-coil and osmotically induced changes in phospholipid composition. *J Biol Chem*. 2005;280(50):41387–94.
- Romantsov T, Helbig S, Culham DE, Gill C, Stalker L, Wood JM. Cardiolipin promotes polar localization of osmosensory transporter ProP in *Escherichia coli*. *Mol Microbiol*. 2007;64(6):1455–65.
- Kannaiah S, Livny J, Amster-Choder O. Spatiotemporal Organization of the Transcriptome: Translation Independence and Engagement in Regulation. *Mol Cell*. 2019;76(4):574–89.
- Laloux G, Jacobs-Wagner C. How do bacteria localize proteins to the cell pole? *J Cell Sci*. 2014;127(1):11–9.
- Oh D, Yu Y, Lee H, Jeon J-H, Wanner BL, Ritchie K. Asymmetric polar localization dynamics of the serine chemoreceptor protein Tsr in *Escherichia coli*. *PLoS ONE*. 2018;13(5):e0195887.
- Erni B. The bacterial phosphoenolpyruvate: sugar phosphotransferase system (PTS): an interface between energy and signal transduction. *J Iran Chem Soc*. 2013;10:593–630.
- Geiser M, Cébe R, Drewello D, Schmitz R. Integration of PCR fragments at any specific site within cloning vectors without the use of restriction enzymes and DNA ligase. *Biotechniques*. 2001;31(1):88–92.
- Datsenko KA, Wanner BL. One-step inactivation of chromosomal genes in *Escherichia coli* K-12 using PCR products. *Proc Natl Acad Sci*. 2000;97(12):6640–5.
- Baba T, Ara T, Hasegawa M, Takai Y, Okumura Y, Baba M, et al. Construction of *Escherichia coli* K-12 in-frame, single-gene knockout mutants: the Keio collection. *Molecular systems biology*. 2006;2(1):2006.0008.
- Kim J, Lee S, Darlington AP, Kim J. Impact of fleQ Gene Expression on Resource Allocation and Heterologous Gene Expression in *Pseudomonas putida* Across Various Growth Media. *Microb Biotechnol*. 2024;17(11):e70054.
- Hong J-C, Fan H-C, Yang P-J, Lin D-W, Wu H-C, Huang H-C. Localized proteolysis for the construction of intracellular asymmetry in *Escherichia coli*. *ACS Synth Biol*. 2021;10(8):1830–6.
- Cooper S. Synthesis of the cell surface during the division cycle of rod-shaped, gram-negative bacteria. *Microbiol Rev*. 1991;55(4):649–74.
- Muthusamy S, Lundin D, Mamede Branca RM, Baltar F, González JM, Lehtiö J, et al. Comparative proteomics reveals signature metabolisms of exponentially growing and stationary phase marine bacteria. *Environ Microbiol*. 2017;19(6):2301–19.
- Bathke J, Konzer A, Remes B, McIntosh M, Klug G. Comparative analyses of the variation of the transcriptome and proteome of *Rhodobacter sphaeroides* throughout growth. *BMC Genomics*. 2019;20:1–13.
- Pletnev P, Osterman I, Sergiev P, Bogdanov A, Dontsova O. Survival guide: *Escherichia coli* in the stationary phase. *Acta Naturae*. 2015;7(4 (27)):22–33.
- Kültz D. Molecular and evolutionary basis of the cellular stress response. *Annu Rev Physiol*. 2005;67:225–57.
- Kim SK, Seong W, Han GH, Lee D-H, Lee S-G. CRISPR interference-guided multiplex repression of endogenous competing pathway genes for redirecting metabolic flux in *Escherichia coli*. *Microb Cell Fact*. 2017;16:1–15.
- Hudson EP. Synthetic biology in cyanobacteria and applications for biotechnology. *Cyanobacteria Biotechnology*. 2021:123–70.
- Wu X, Cai P, Yao L, Zhou YJ. Genetic tools for metabolic engineering of *Pichia pastoris*. *Engineering Microbiology*. 2023:100094.
- Thanbichler M, Shapiro L. Getting organized—how bacterial cells move proteins and DNA. *Nat Rev Microbiol*. 2008;6(1):28–40.

42. Barák I, Muchová K. The role of lipid domains in bacterial cell processes. *Int J Mol Sci*. 2013;14(2):4050–65.
43. Irastortza-Olaziregi M, Amster-Choder O. RNA localization in prokaryotes: where, when, how, and why. *Wiley Interdisciplinary Reviews: RNA*. 2021;12(2): e1615.
44. Fazal FM, Han S, Parker KR, Kaewsapsak P, Xu J, Boettiger AN, et al. Atlas of subcellular RNA localization revealed by APEX-Seq. *Cell*. 2019;178(2):473–90. e26.
45. Serres MH, Gopal S, Nahum LA, Liang P, Gaasterland T, Riley M. A functional update of the *Escherichia coli* K-12 genome. *Genome Biol*. 2001;2:1–7.
46. Albicoro FJ, Vacca C, Cañero JH, Draghi WO, Martini MC, Goulian M, et al. Comparative Proteomic Analysis Revealing ActJ-Regulated Proteins in *Sinorhizobium meliloti*. *Journal of Proteome Research*. 2023.
47. Vaquerizas JM, Suyama R, Kind J, Miura K, Luscombe NM, Akhtar A. Nuclear pore proteins nup153 and megator define transcriptionally active regions in the *Drosophila* genome. *PLoS Genet*. 2010;6(2): e1000846.
48. van Steensel B, Furlong EE. The role of transcription in shaping the spatial organization of the genome. *Nat Rev Mol Cell Biol*. 2019;20(6):327–37.
49. Chen XJ, Wang B, Thompson IP, Huang WE. Rational design and characterization of nitric oxide biosensors in *E. coli Nissle* 1917 and mini SimCells. *ACS Synthetic Biology*. 2021;10(10):2566–78.
50. Chen JX, Steel H, Wu Y-H, Wang Y, Xu J, Rampley CP, et al. Development of aspirin-inducible biosensors in *Escherichia coli* and SimCells. *Appl Environ Microbiol*. 2019;85(6):e02959–e3018.
51. Sourjik V, Armitage JP. Spatial organization in bacterial chemotaxis. *EMBO J*. 2010;29(16):2724–33.
52. Linnik D, Maslov I, Punter CM, Poolman B. Dynamic structure of *E. coli* cytoplasm: supramolecular complexes and cell aging impact spatial distribution and mobility of proteins. *Communications biology*. 2024;7(1):508.
53. Allen S, Polazzi JO, Gierse J, Easton A. Two novel heat shock genes encoding proteins produced in response to heterologous protein expression in *Escherichia coli*. *J Bacteriol*. 1992;174(21):6938–47.
54. Lindner AB, Madden R, Demarez A, Stewart EJ, Taddei F. Asymmetric segregation of protein aggregates is associated with cellular aging and rejuvenation. *Proc Natl Acad Sci*. 2008;105(8):3076–81.
55. Rang CU, Proenca A, Buetz C, Shi C, Chao L. Minicells as a damage disposal mechanism in *Escherichia coli*. *Mosphere*. 2018;3(5):<https://doi.org/10.1128/msphere.00428-18>.
56. Shi C, Chao L, Proenca AM, Qiu A, Chao J, Rang CU. Allocation of gene products to daughter cells is determined by the age of the mother in single *Escherichia coli* cells. *Proc R Soc B*. 1926;2020(287):20200569.
57. Lai EM, Nair U, Phadke ND, Maddock JR. Proteomic screening and identification of differentially distributed membrane proteins in *Escherichia coli*. *Mol Microbiol*. 2004;52(4):1029–44.
58. Proenca AM, Rang CU, Qiu A, Shi C, Chao L. Cell aging preserves cellular immortality in the presence of lethal levels of damage. *PLoS Biol*. 2019;17(5): e3000266.
59. Coquel A, Jacob J, Primet M, Demarez A, Dimiccoli M. Localization of Protein Aggregation in *Escherichia coli* Is Governed by Diffusion. 2013.
60. Lybarger SR, Maddock JR. Polarity in action: asymmetric protein localization in bacteria. *J Bacteriol*. 2001;183(11):3261–7.
61. Nevo-Dinur K, Nussbaum-Shochat A, Ben-Yehuda S, Amster-Choder O. Translation-independent localization of mRNA in *E. coli*. *Science*. 2011;331(6020):1081–4.
62. Sheng HJ, Stauffer WT, Hussein R, Lin C, Lim HN. Nucleoid and cytoplasmic localization of small RNAs in. *Nucleic Acids Res*. 2017;45(5):2919–34.
63. Saberi S, Emberly E. Non-equilibrium polar localization of proteins in bacterial cells. *PLoS ONE*. 2013;8(5): e64075.
64. Stylianidou S, Kuwada NJ, Wiggins PA. Cytoplasmic dynamics reveals two modes of nucleoid-dependent mobility. *Biophys J*. 2014;107(11):2684–92.
65. Neeli-Venkata R. The Role of Nucleoid Exclusion in the Intracellular Spatial Organization of *Escherichia coli*. 2017.
66. Romantsov T, Helbig S, Culham DE, Gill C, Stalker L, Wood JM. Cardiolipin promotes polar localization of osmosensory transporter ProP in. *Mol Microbiol*. 2007;64(6):1455–65.
67. Romantsov T, Battle AR, Hendel JL, Martinac B, Wood JM. Protein localization in *Escherichia coli* cells: comparison of the cytoplasmic membrane proteins ProP, LacY, ProW, AqpZ, MscS, and MscL. *J Bacteriol*. 2010;192(4):912–24.
68. Kannaiah S, Goldberger O, Alam N, Barnabas G, Pozniak Y, Nussbaum-Shochat A, et al. MinD-RNase E interplay controls localization of polar mRNAs in *E. coli*. *The EMBO Journal*. 2024;43(4):637–62.
69. Govindarajan S, Elisha Y, Nevo-Dinur K, Amster-Choder O. The general phosphotransferase system proteins localize to sites of strong negative curvature in bacterial cells. *MBio*. 2013;4(5):<https://doi.org/10.1128/mbio.00443-13>.
70. Bi S, Sourjik V. Stimulus sensing and signal processing in bacterial chemotaxis. *Curr Opin Microbiol*. 2018;45:22–9.
71. Barrows JM, Goley ED. Synchronized swimmers and sticky stalks: *Caulobacter crescentus* as a model for bacterial cell biology. *J Bacteriol*. 2023;205(2):e00384–e422.
72. Lin D-W, Liu Y, Lee Y-Q, Yang P-J, Ho C-T, Hong J-C, et al. Construction of intracellular asymmetry and asymmetric division in *Escherichia coli*. *Nat Commun*. 2021;12(1):888.
73. Ebersbach G, Briegel A, Jensen GJ, Jacobs-Wagner C. A self-associating protein critical for chromosome attachment, division, and polar organization in *caulobacter*. *Cell*. 2008;134(6):956–68.
74. Laloux G, Jacobs-Wagner C. Spatiotemporal control of PopZ localization through cell cycle-coupled multimerization. *J Cell Biol*. 2013;201(6):827–41.
75. Nordyke CT, Ahmed YM, Puterbaugh RZ, Bowman GR, Varga K. Intrinsically disordered bacterial polar organizing protein Z, PopZ, interacts with protein binding partners through an N-terminal Molecular Recognition Feature. *J Mol Biol*. 2020;432(23):6092–107.
76. Holmes JA, Follett SE, Wang H, Meadows CP, Varga K, Bowman GR. *Caulobacter* PopZ forms an intrinsically disordered hub in organizing bacterial cell poles. *Proc Natl Acad Sci*. 2016;113(44):12490–5.
77. Silva-Rocha R, Martínez-García E, Calles B, Chavarría M, Arce-Rodríguez A, de Las HA, et al. The Standard European Vector Architecture (SEVA): a coherent platform for the analysis and deployment of complex prokaryotic phenotypes. *Nucleic Acids Res*. 2013;41(D1):D666–75.

Publisher's Note

Springer Nature remains neutral with regard to jurisdictional claims in published maps and institutional affiliations.